CrossMark

Effects of aerosol on evaporation, freezing and precipitation in a multiple cloud system

Seoung Soo Lee[1] · Byung-Gon Kim[2] · Seong Soo Yum[3] · Kyong-Hwan Seo[4] ·
Chang-Hoon Jung[5] · Jun Shik Um[6] · Zhanqing Li[1] · JinKyu Hong[3] · Ki-Ho Chang[7] ·
Jin-Yim Jeong[7]

Abstract Aerosol effects on clouds and precipitation account for a large portion of uncertainties in the prediction of the future course of global hydrologic circulations and climate. As a process of a better understanding of interactions between aerosol, clouds and precipitation, simulations are performed for a mixed-phase convective multiple-cloud system over the tropics. Studies on single-cloud systems have shown that aerosol-induced increases in freezing, associated increases in parcel buoyancy and thus the intensity of clouds (or updrafts) are a main mechanism which controls aerosol–cloud–precipitation interactions in convective clouds. However, in the multiple-cloud system that plays much more important roles in global hydrologic circulations and thus climate than single-cloud systems, aerosol effects on condensation play the most important role in aerosol-induced changes in the intensity of clouds and the effects on freezing play a negligible role in those changes. Aerosol-induced enhancement in evaporation intensifies gust fronts and increases the number of subsequently developing clouds, which leads to the substantial increases in condensation and associated intensity of convection. Although aerosol-induced enhancement in freezing takes part in the increases in condensation by inducing stronger convergence around cloud bottom, the increases in condensation are ~one order of magnitude larger than those in freezing. It is found that while aerosol-induced increases in freezing create intermittent extremely heavy precipitation, aerosol-induced increases in evaporation enhance light and medium precipitation in the multiple-cloud system here. This increase in light and medium precipitation makes it possible that cumulative precipitation increases with increasing aerosol concentration, although the increase is small. It is interesting that the altitude of the maximum of the time- and domain-averaged hydrometeor mass densities is quite robust to increases in aerosol concentration. This is because locations of gust fronts and homogeneous freezing do not vary significantly with changing aerosol concentration and this outweighs aerosol effects on hydrometeor size.

Keywords Aerosol · Evaporation · Freezing · Convective clouds · Precipitation

✉ Seoung Soo Lee
cumulss@gmail.com; slee1247@umd.edu

1 Earth System Science Interdisciplinary Center, University of Maryland, College Park, Maryland, USA

2 Department of Atmospheric Environmental Sciences, Gangneung-Wonju National University, Gangneung, Gang-Won do, South Korea

3 Department of Atmospheric Sciences, Yonsei University, Seoul, South Korea

4 Department of Atmospheric Sciences, Pusan National University, Pusan, South Korea

5 Department of Health Management, Kyungin Women's Univesity, Incheon, South Korea

6 Department of Atmospheric Sciences, University of Illinois at Urbana-Champaign, Urbana, Illinois, USA

7 National Institute of Meteorological Sciences, Seoul, South Korea

1 Introduction

In recent years, aerosol effects on clouds and precipitation in the systems of convective clouds have been the focus of studies on aerosol–cloud–precipitation interactions. Convective clouds form the cloud regime that produces most of the precipitation on a global average basis, and so are

important for determining the relationship between aerosol and precipitation and thus the effect of the relationship on global hydrologic circulations and climate.

So far, most of studies have focused on aerosol-induced changes in precipitation amount (or cumulative precipitation) in convective clouds (e.g., Khain et al. 2005; Lee et al. 2010; Lee 2011). Some of these studies for mesoscale cloud ensembles (MCEs) have shown that precipitation amount over the entire domain does not change much with varying aerosol concentrations. However, Lee et al. (2010), referred to as L10, hereafter, have shown that aerosol-induced precipitation-amount changes in each of classified cloud types in a simulated MCE are significant, while the compensation of aerosol-induced precipitation-amount changes among the different cloud types results in the small variation of precipitation amount over the entire MCE domain. Motivated by L10, this study examines aerosol-induced changes in precipitation and associated changes in clouds for quantified cloud types. In this study, cloud types are quantified or classified by cloud depths.

Despite the small aerosol-induced deviation in precipitation amount over the entire MCE domain, Li et al. (2011) have shown aerosol-induced significant changes in precipitation frequency (PF). This study suggests that we should shift our focus from precipitation amount to PF to gain a more comprehensive understanding of aerosol effects on precipitation in convective clouds. Also, as discussed in Li et al. (2011), changes in PF can have a substantial impact on water usage efficiency, an important element for agriculture. Motivated by this, this study aims to understand mechanisms which control interactions between aerosol and PF. For the understanding of the mechanisms, this study focuses on roles played by latent-heat processes (e.g., evaporation and freezing) and associated cloud dynamics in the interactions between aerosol and PF, since it is well-known that those latent-heat processes and cloud dynamics play a key role in the evolution of precipitation and aerosol effects on it (Lee et al. 2009; Rosenfeld et al. 2008; Houze 1993).

The traditional understanding of the interactions between aerosol and clouds is based on aerosol-induced changes in microphysical effects on clouds, which involve aerosol-induced changes on cloud-particle sizes (Zhao et al. 2012; Garrett and Zhao 2006; Albrecht 1989; Twomey 1977). With the focus of this study on dynamics, this study compares the traditional effects of aerosol-induced changes in microphysics on the interactions between aerosol and clouds to those effects of aerosol-induced changes in cloud dynamics. The traditional roles played by aerosol-induced changes in microphysics have been investigated and well-understood in the vertical structure of hydrometeors (e.g., the vertical distribution of hydrometeor mass). Based on this, as a process of the effective comparison, this

study aims to elucidate how the well-understood effects of aerosol-induced changes in microphysics on the vertical structure are deformed by those effects of aerosol-induced changes in cloud dynamics. In particular, for the elucidation regarding the vertical structure of cloud-ice (or ice-crystal) mass, we also discuss the roles in the deformation played by environmental conditions (e.g., large-scale forcings) and their collaboration with aerosol-induced changes in cloud dynamics. This elucidation gives us information of how important cloud dynamics is in our understanding of aerosol effects on clouds and precipitation.

In Sects. 2 and 3, the cloud-system resolving model (CSRM) and integration design are described and in Sect. 4, analyses of simulation results are presented. In Sect. 5, the discussion of the results in this study is given and in Sect. 6, a summary of the results and conclusions are given. In particular, in Sects. 4.1 and 4.2, the results that are associated with the effect of aerosol on latent-heat processes, clouds and precipitation are presented. In Sect. 4.3, the results that are related to the elucidation of how the effects of aerosol-induced changes in microphysics on the vertical distribution of hydrometeor mass are affected by those effects of large-scale forcings and aerosol-induced changes in dynamics are given.

2 CSRM

The Goddard Cumulus Ensemble (GCE) model (Tao et al. 2003), a two-dimensional nonhydrostatic compressible model, is used here as a CSRM. Shortwave and longwave radiation parameterizations have been included for simulations in this study. To represent the subgrid turbulent processes, 1.5 order turbulent kinetic energy closure that is described in Mellor and Yamada (1982) is used. Microphysical processes are represented by the double-moment bin-bulk representation of Saleeby and Cotton (2004) that uses bin-model-derived lookup tables for hydrometeor collection processes. Hydrometeor size distributions are assumed to be gamma functions with fixed breadth. The cloud-droplet nucleation parameterization of Abdul-Razzak and Ghan (2000, 2002), which is based on Köhler theory, is used to represent cloud-droplet nucleation. Arbitrary aerosol mixing states and arbitrary aerosol size distributions can be fed to this parameterization because it combines the treatment of multiple aerosol types and a sectional representation of size. To represent heterogeneous ice-crystal nucleation, the parameterizations of Lohmann and Diehl (2006) and Möhler et al. (2006) are used. In these parameterizations, contact, immersion, condensation-freezing, and deposition nucleation paths are all considered. In this study, cloud-liquid (or cloud droplet) and raindrop heterogeneous freezing occurs through immersion

and contact freezing following Lohmann and Diehl (2006) and Möhler et al. (2006). Homogeneous aerosol (haze particle) freezing is considered following the theory of Koop et al. (2000). Homogeneous aerosol (haze particle) freezing is assumed to occur instantaneously when a size- and temperature-dependent critical supersaturation with respect to ice for the freezing is exceeded at temperatures colder than −38 °C. For homogeneous droplet freezing, the fraction by number of cloud droplets that are frozen homogeneously just above the level of −38 °C is parameterized as a function of the vertical velocity, the predicted supersaturation at the level just below the homogeneous freezing, and the product of droplet number concentration and size, following Phillips et al. (2007a). In applying these droplet and ice-crystal nucleation parameterizations, the size spectrum for aerosols (described in more detail in Sect. 3) is divided into thirty bins.

Prognostic equations are solved for aerosol. Aerosol particles are advected, diffused and depleted by activation and washout by precipitable hydrometeors (i.e., nucleation and impacting scavenging) during the simulation. Note that Garrett et al. (2010), Pruppacher and Klett (1997), and Shaw (1995) have shown that the washout of aerosol by precipitating hydrometeors or precipitation is proportional to the intensity of precipitation or precipitation rates based on measurements and experiments. This principle is operative in the simulation of the washout in this study. Aerosol mass is incorporated into hydrometeors during droplet or ice nucleation and is transferred among different species of hydrometeors (through collection). The aerosol is removed from the system when precipitating hydrometeors fall to the surface or returned to the atmosphere when hydrometeors evaporate or sublimate.

We do not simulate the solar absorption of black-carbon aerosol and attendant effects on the strength of convection and regional circulation.

3 Integration design

A 2-day simulation is performed for a MCE that was observed during the TWP-ICE [12:00 local solar time (LST) January 23th–12:00 LST January 25th 2006] campaign in Darwin, Australia (12.47°N, 130.85°W) (May et al. 2008). Henceforth, this simulation is referred to as the "control run".

The horizontal domain length is set to 256 km in the east–west direction to capture the mesoscale structure of the storm while the vertical extent is 20 km. The horizontal (vertical) grid length is 500 (200) m.

Periodic boundary conditions used in Fridlind et al. (2009) are applied to horizontal boundaries, and heat and moisture fluxes from the TWP-ICE observation are
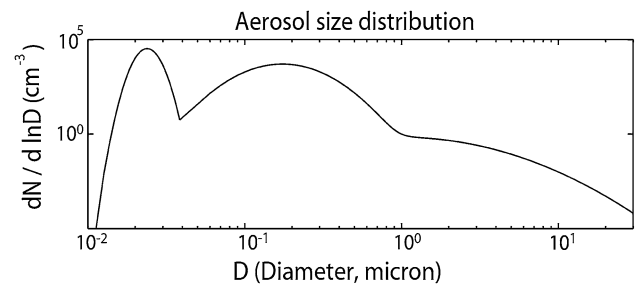
Fig. 1 Initial aerosol size distribution at the altitude of 0.5 km. N represents aerosol number concentration per unit volume of air and D aerosol diameter
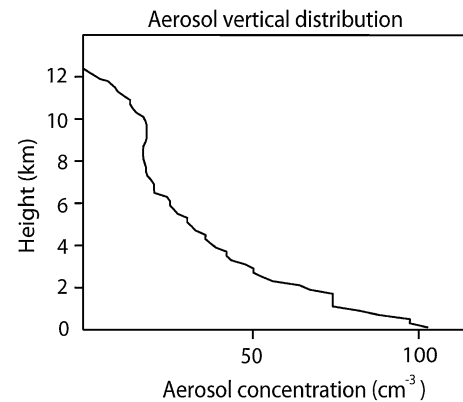
Fig. 2 Initial vertical distribution of aerosol concentration in the accumulation mode for the control run

prescribed at the surface. The TWP-ICE observations provide large-scale forcings, in terms of advection of potential temperature and specific humidity, which control the net water budget over the domain but not the cloud-scale microphysics directly. This allows us to explore the change in microphysical pathways associated with changes in aerosol. Horizontal momentum is damped to observed values.

The initial size distribution and number concentration of background aerosol are shown in Fig. 1. Figure 1 is only for the altitude of 0.5 km. Modal diameter and distribution breadth of each of modes of the size distribution are assumed not to vary spatiotemporally, hence, aerosol particles in any grid points have the shape of the size distribution in Fig. 1, although their total number concentration varies spatiotemporally due to clouds that process aerosol particles as described in Sect. 2. Here, a chemical composition, which is ammonium sulfate, is assumed for all of aerosol particles over the whole simulation domain and period. Hence, we do not consider the effect of varying composition on clouds and precipitation. The initial average background aerosol number concentration in the accumulation mode which has most of CCN over a general

parcel supersaturation range and over the planetary boundary layer is ~100 cm^{-3}. Figure 2 depicts the initial vertical distributions of aerosol concentrations in the accumulation mode for the control run.

To examine the effect of aerosol on precipitation, the control run is repeated but with the initial background aerosol number enhanced by a factor of 10 over the control case. Henceforth, this simulation is referred to as "the 10M run". To test the robustness of results to a lower aerosol perturbation, the control run is repeated with aerosol number concentration enhanced by a factor of 3. This repeated simulation is referred to as "the 3M run".

4 Results

4.1 Cumulative precipitation

The domain-averaged cumulative precipitation at the last time step is 88.6, 90.1 mm and 95.7 mm for the control, 3M and 10M runs, respectively. The observed cumulative precipitation is 83.1 mm, hence, the control-run precipitation amount is within 10 % of the observed precipitation amount, which indicates that the model performs reasonably well. The cumulative precipitation in the 3M and 10M runs exceeds that in the control run only by less than ~9 % in spite of as much as the tenfold difference in aerosol concentration between the control run and the 10M run or the threefold difference between the control run and the 3M run. This is due to offset between cloud types as described in L10.

4.2 PF, cloud depths and cloud fraction

4.2.1 Aerosol effects on PF

Although variations in cumulative precipitation between the three runs are very small, the distribution of PF over precipitation rate (R) show features which clearly differentiates the 3M and 10M runs from the control run (Fig. 3a). PF is the number of the occurrence of a certain R over the whole domain and simulation period. The notable difference in the PF distribution between the runs is in R exceeding ~28 mm h^{-1}. While the 3M and 10M runs show non-zero PFs, there are zero PFs in the control run for R over ~28 mm h^{-1}. Also, it is notable that for R below ~5 mm h^{-1}, the 3M and 10M runs show on average ~20 and 30 % larger PFs than the control run, while the control run shows on average ~22 and 35 % larger PFs than the 3M and 10M runs, respectively, for the R between ~5 and ~15 mm h^{-1}. For R between ~15 and ~28 mm h^{-1}, the 3M and 10M runs show 25 and ~40 % larger PFs than the control run on average, respectively. The 3M and 10M runs

respond to the aerosol perturbation in a qualitatively similar way (Fig. 3a, discussions in this section, as well as further analyses in subsequent sections). Hence, results from the 10M and control runs will hereafter be the focus of analysis and discussion.

The differences in PF between the 10M and control runs may have been caused by the 9 % difference in cumulative precipitation, although it is not likely that this small precipitation-amount difference has a significant impact on them. To see the effect of this precipitation-amount difference on the PF differences, the 10M run is repeated by artificially slowing down the graupel collection of cloud liquid such that this repeated 10M run results in similar cumulative precipitation to that in the control run. Among many types of collection processes, this graupel collection is chosen here, since it is well known that this collection has the very efficient control on the total rainfall. This run is referred to as the 10M-9 % run. The general features of the PF differences between the 10M-9 % and control runs are similar to those between the 10M and control runs, although PF decreases slightly in the 10M-9 % run as compared to PF in the 10M run (Fig. 3b). Hence, the features of differences in PF over R can be considered robust to the precipitation-amount difference between the 10M and control runs.

4.2.2 Freezing and evaporation

There are two well-established mechanisms which cause aerosol-induced changes in convective intensity and precipitation. The first is aerosol-induced increases in freezing (as simulated in the 10M run) and the second is aerosol-induced increases in evaporation (as also simulated in the 10M run). Aerosol-induced increases in freezing lead to increases in parcel buoyancy as proposed by studies such as Rosenfeld et al. (2008) and this triggers stronger convergence around cloud bottoms, in turn inducing larger updrafts and thus larger condensation. In this paper, freezing is defined to include all types of microphysical processes which convert liquid- and gas-phase particles to solid-phase particles. Hence, freezing here involves processes of cloud-liquid (or cloud-droplet) freezing, raindrop freezing, depositional growth of cloud ice (or ice crystals), snow and graupel, riming of liquid-phase particles by their collisions with solid-phase particles and heterogeneous and homogeneous cloud-ice nucleation. Note that deposition processes are included in freezing here and this enables us to consolidate all the ice processes forming solid particles into one term, which is freezing, and thus to achieve the expediency of explaining those processes.

Aerosol-induced increases in evaporation that induce the enhancement of the intensity of gust fronts (or convergence around the surface) increase the number of
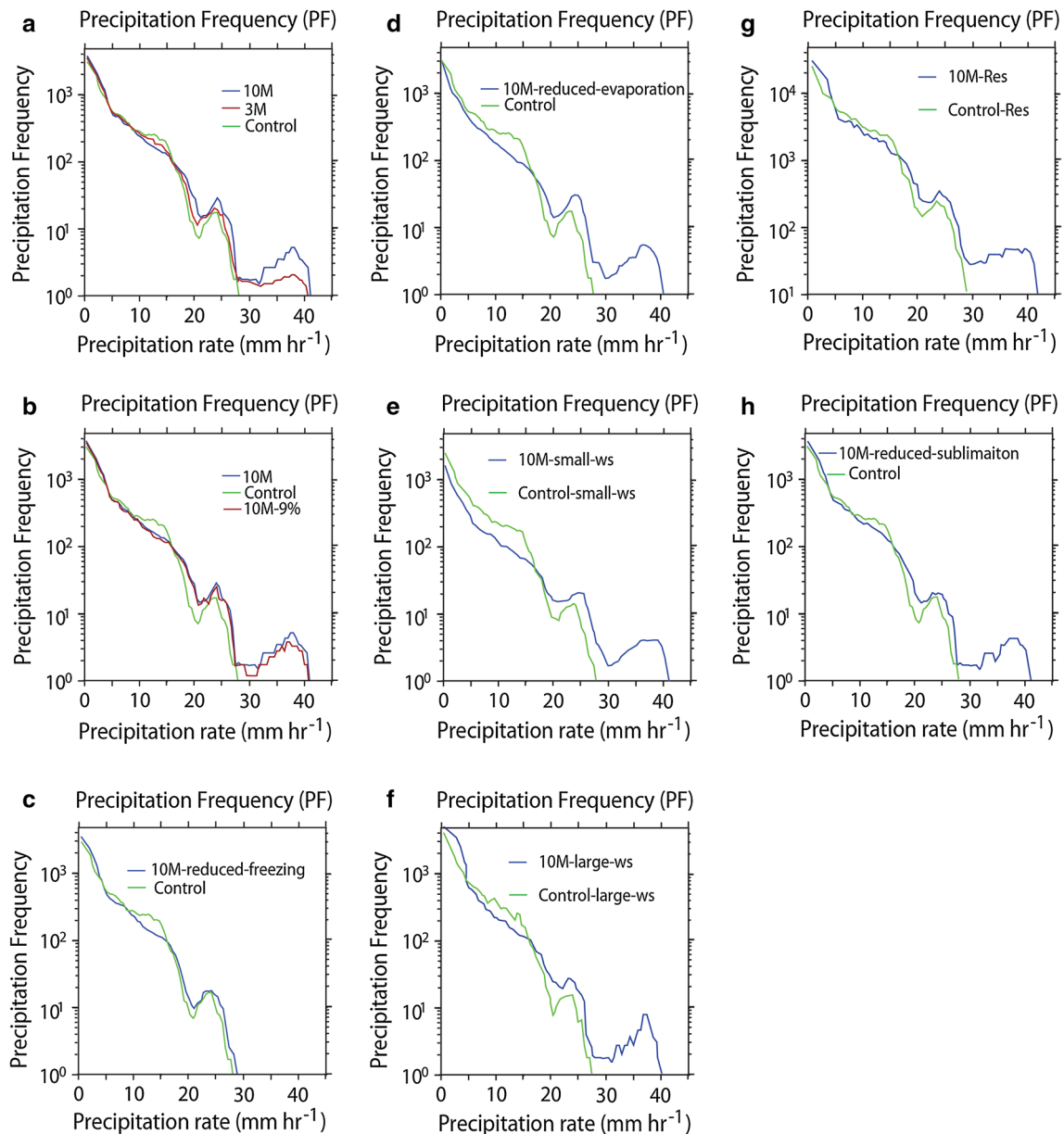
Fig. 3 Distributions of precipitation-rate (R) frequency for **a** the 3M, 10M and control runs, **b** the 10M, control and 10M-9 % runs, **c** the 10M-reduced-freezing and control runs, **d** the 10M-reduced-evapora-tion and control runs, **e** the 10M-small-ws and control-small-ws runs, **f** the 10M-large-ws and control-large-ws runs, **g** the 10M-res and control-res runs and **h** the 10M-reduced-sublimation and control runs

subsequently developing updraft cores and thus clouds (or cloud cells), contributing to the substantial increases in the averaged updrafts and condensation as identified by studies such as Khain et al. (2005) and L10 and diagram-matically described in Fig. 4a. Due to these effects of aer-osol-induced increases in evaporation on gust fronts, the cumulative numbers of cloud cells and updrafts cores at the last time step are larger in the 10M run than in the control run. The cumulative numbers of cloud cells and updrafts cores at the last time step for the 10M run (control run) are 909 (719) and 2728 (2085), respectively.

As seen in Table 1, aerosol-induced increases in con-densation are ~one order of magnitude larger than the increases in freezing. Also, as seen in Table 1, increases in condensation as a source of cloud liquid are slightly larger than those in evaporation as a sink of cloud liquid. As dis-cussed in Eqs. (6) and (7) in Lee et al. (2008a), this induces increases in cloud-liquid mass and thus accretion of cloud liquid by precipitation, which offset decreases in autocon-version in the 10M run, and eventually enables slightly larger cumulative precipitation in the 10M run than in the control run. Hence, we see that although aerosol-induced
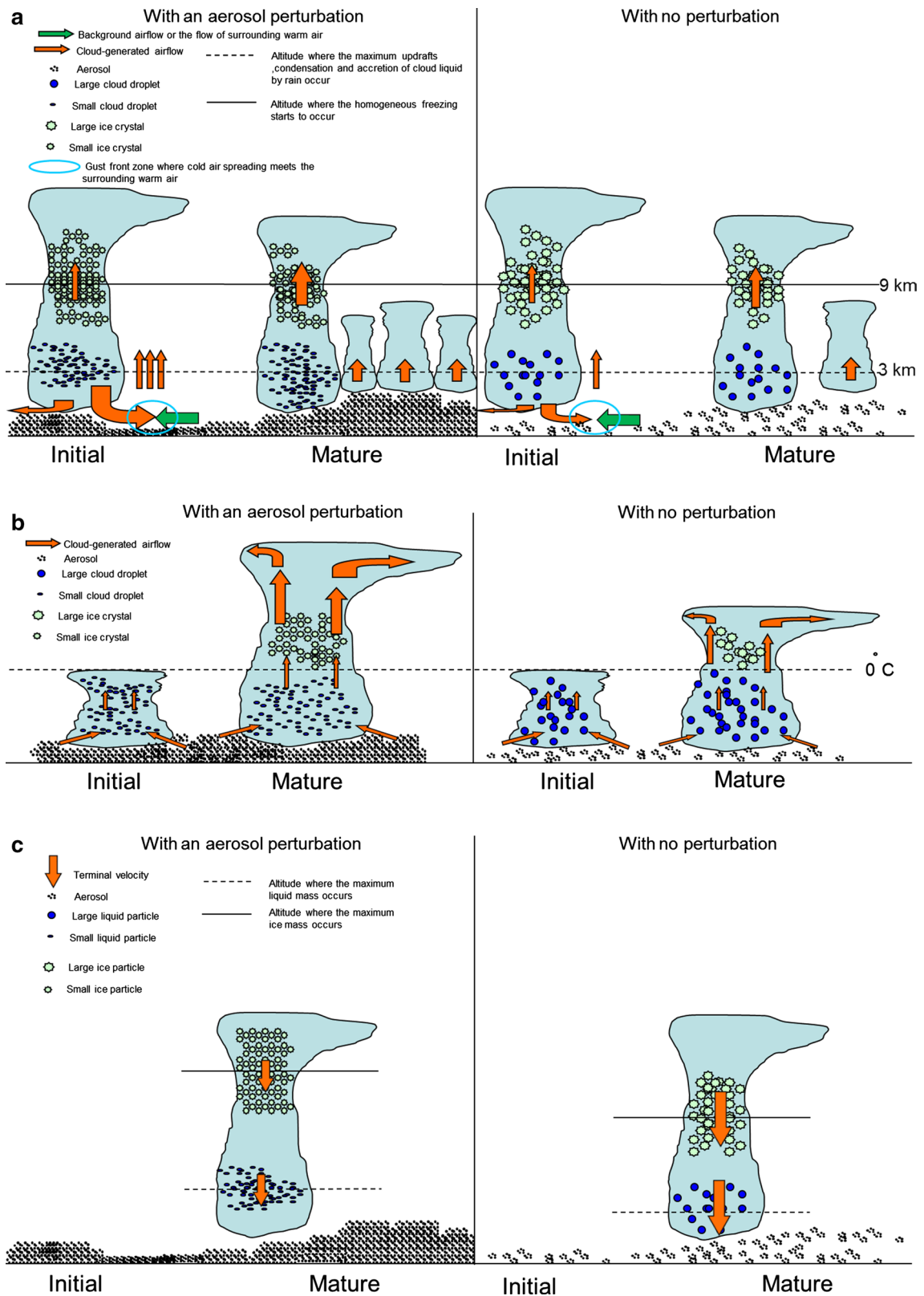
increases in freezing trigger those in condensation, the increases in freezing and its latent heat play a negligible role in the invigoration of convection as compared to those

in condensation and its latent heat. We can also see that although there are substantial increases in evaporation and thus the loss of cloud mass as a source of precipitation with

Fig. 4 a A diagram that depicts aerosol-induced intensification of gust fronts and formation of more subsequent clouds. Aerosol-induced increases in evaporation develop stronger downdrafts and outflow around the surface, in turn developing stronger gust fronts. This leads to the formation of more clouds in the perturbed regions. This diagram also depicts the occurrence of the maximum cloud-ice number concentration and aerosol-induced increases in homogeneous freezing around the level of homogeneous freezing. **b** A diagram that depicts aerosol-induced deeper growth of clouds. An aerosol perturbation stimulates the formation of smaller size but larger number of water droplets in the lower layers of convective clouds. This, in turn, leads to the transportation of a greater number of water droplets upwards, and the formation and growth of more ice crystals in the upper cloud layers. The more latent heat energy released upon more ice crystal formation and growth stimulates the deeper growth of clouds in the perturbed regions. **c** A diagram that depicts the dependence of the terminal velocity of cloud particles on the particle size. Aerosol-induced decreases in the particle size induce the smaller terminal velocity of particles and this tends to make particles stay at higher altitudes

the increasing aerosol, these increases in evaporation also act to intensity gust fronts and thus subsequent clouds, in turn increasing condensation as a source of precipitation.

4.2.3 Test simulations for evaporation and freezing

To better understand the effects of aerosol-induced changes in freezing and evaporation on clouds and precipitation, we perform test simulations. For the test simulations, first, the 10M run is repeated by reducing the freezing rate to examine the effect of aerosol-induced increases in freezing on the PF differences between the 10M run and the control run. This is done by dividing the rate of each of freezing processes (i.e., cloud-liquid and raindrop freezing, depositional growth of cloud ice, snow and graupel, riming of liquid-phase particles by their collisions with solid-phase particles and heterogeneous and homogeneous nucleation) by a factor of 7 at every time step and at grid points where freezing occurs. This factor is determined to make cumulative freezing in the repeated 10M run identical to that in the control run. This repeated run is referred to as "the 10M-reduced-freezing run". As seen in Fig. 3c, the 10M-reduced-freezing run does not have extremely heavy precipitation above ~28 mm h^{-1}, which is in contrast to the 10M run. Also, the

Table 1 Cumulative sources of four phase-transition processes, averaged over the domain at the last time step

Simulations	Condensation (mm)	Evaporation (mm)	Freezing (including deposition) (mm)	Sublimation (mm)
Control	174	92	18	11
10M	240	147	25	17
10M minus control	66	55	7	6

PF differences between the 10M-reduced-freezing and control runs in R above ~15 mm h^{-1} is overall ~2 times smaller than that between the 10M and control runs (Fig. 3a and c). Note that PFs in Fig. 3a and c are in log scales so that seemingly slight changes in the PF differences in these figures can be large in absolute values. However, for R below 15 mm h^{-1}, changes in the PF differences with the suppressed freezing are ~3 times smaller than those for R above 15 mm h^{-1} (Fig. 3a and c). Hence, aerosol-induced changes in freezing affect heavy precipitation, defined to have rates above 15 mm h^{-1}, more significantly.

The 10M run is repeated again by reducing evaporation rate to examine the effect of aerosol-induced increases in evaporation on the PF differences between the 10M run and the control run. Evaporation rate at grid points where evaporation occurs is reduced by a factor of 1.5 which is determined to make cumulative evaporation in the repeated run identical to that in the control run. This repeated run is referred to as "the 10M-reduced-evaporation run". Figure 3a and d show that there is a small ~5 % increase in PF with the suppressed evaporation for R above ~15 mm h^{-1} as compared to PF in the 10M run. Hence, PF for R above ~15 mm h^{-1} in this repeated run is larger than that in the control run as in the 10M run, which indicates that the qualitative nature of the effect of the aerosol perturbation on PF for R above ~15 mm h^{-1} does not vary with increasing evaporation which is induced by increasing aerosol. However, there is ~30 % decrease in PF with the suppressed evaporation as compared to that in the 10M run for R below ~15 mm h^{-1} (Fig. 3a and d). As a result of this, for R below 5 mm h^{-1}, PF in the high-aerosol case becomes smaller than PF in the low-aerosol case with the reduced evaporation (Fig. 3a and d). Hence, in contrast to the role of freezing, aerosol-induced enhancement in evaporation increases the occurrence of light and medium precipitation with R below 15 mm h^{-1} more significantly. Light precipitation is defined to have rates below 5 mm h^{-1}, while medium precipitation is defined to have rates between 5 and 15 mm h^{-1} in this study. The cumulative precipitation at the last time step is 80.7 mm for the 10M-reduced-evaporation run which is smaller than 88.6 mm in the control run. Hence, despite the small R in light and medium precipitation, the increase in the occurrence of light and medium precipitation (induced by aerosol-induced increases in evaporation) enhances cumulative precipitation significantly. This enhancement of cumulative precipitation (associated with light and medium precipitation) enables the slightly larger cumulative precipitation in the 10M run than in the control run. The cumulative precipitation in the 10M-reduced-freezing run is 94.2 mm which is higher than that in the control run. Hence, aerosol-induced increases in freezing do not have an impact on cumulative precipitation as strong as aerosol-induced increases in evaporation.
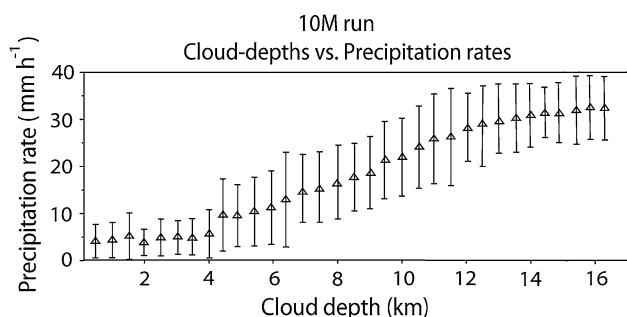
Fig. 5 R corresponding to each cloud depth for the 10M run. *Vertical bars* represent ± one standard deviation of R at each of discretized cloud depths

4.2.4 Aerosol effects on cloud depths and cloud fraction

Figure 5 depicts the precipitation-rate distribution over cloud depths for the 10M run. There are only less than 10 % differences in the precipitation-rate distribution between the control and 10M runs for each of cloud depths, although the control-run cloud depths exist to ~15 km while the 10M-run depths extend to ~16 km (not shown). This figure shows that generally deeper clouds produce higher R. This figure also roughly shows that, based on the mean R for each cloud depth, clouds with depths smaller than ~4 km tend to produce R below ~5 mm h^{-1}. Clouds with depths between ~4 and ~8 km tend to control R between 5 and 15 mm h^{-1}, while clouds with depths above ~8 km tend to account for R above 15 mm h^{-1}. Figure 6 shows the frequency of cloud depths. Shallow clouds with depths smaller than ~4 km occur more frequently in the 10M run than in the control run (Fig. 6a). However, clouds with depths between ~4 and ~8 km occur more frequently in the control run than in the 10M run (Fig. 6a). For deep clouds with depths larger than ~8 km, clouds in the 10M run occur more frequently than in the control run (Fig. 6a). Taking into account the mean R for each of cloud depths in Figs. 5 and 6a roughly indicate that larger PFs for R below 5 mm h^{-1} are produced by more clouds with depths below ~4 km in the 10M run than in the control run. The larger PFs for R above 15 mm h^{-1} are accounted for by more clouds with depths above ~8 km in the 10M run than in the control run. The larger PFs for R between 5 and 15 mm h^{-1} are from more clouds with depths between ~4 km and ~8 km in the control run than in the 10M run.

The 10M-reduced-freezing run shows a substantial reduction in the frequency of clouds with depths above ~8 km as compared to the frequency in the 10M run (Fig. 6a and b). This explains the reduction in PF for R above 15 mm h^{-1} in the 10M-reduced freezing run as compared to PF in the 10M run (Fig. 3a and c). Aerosol-induced increases in freezing in the 10M run (as compared to the 10M-reduced-freezing run or the control run) increase the occurrence of

clouds with large depths above ~8 km by making clouds grow deeper as proposed by Rosenfeld et al. (2008) and diagrammatically depicted in Fig. 4b. This leads to increases in the occurrence of heavy rain (with rates above 15 mm h^{-1}) in the 10M run as compared to the 10M-reduced-freezing run or the control run. The reduction in clouds with depths above ~8 km is associated with the disappearance of precipitation with the rate above ~28 mm h^{-1} in the 10M-reduced-freezing run. However, this reduction does not change the qualitative nature of aerosol effects on cloud fraction as seen in comparison between Fig. 7a and b; the 10M run and the 10M-reduced-freezing run both show larger cloud fraction than the control run.

The 10M-reduced-evaporation run shows a substantial decrease in clouds with depths below ~8 km as compared to these clouds in the 10M run (Fig. 6a and c). This decrease leads to smaller cloud-depth frequency for cloud depths below ~4 km in the 10M-reduced-evaporation run than in the control run (Fig. 6a and c). This accounts for the substantial reduction in PF for R below 15 mm h^{-1} in the 10M-reduced-evaporation run as compared to PF in the 10M run, which leads to smaller PFs for R below 5 mm h^{-1} in the 10M-reduced evaporation run than in the control run. Here, we see that aerosol-induced increases in evaporation increase the occurrence of clouds with shallow depths below ~8 km as diagrammatically depicted in Fig. 4a. The change in clouds with shallow depths with increasing evaporation are associated with aerosol-induced increases in cloud fraction as seen in comparisons between Fig. 7a and c.

4.2.5 More analyses and discussion of the effects of aerosol-induced changes in evaporation

To examine the effects of aerosol-induced increases in evaporation on PF and cloud-depth frequency distributions in more detail, Fig. 8 that shows the temporal evolution of the domain-averaged differences in updrafts, downdrafts, convergence at the surface and evaporation-related negative buoyancy between the 10M run and the control run is obtained. Aerosol-induced increases in evaporation enhance the negative buoyancy first, which in turn enhances the intensity of downdrafts around 18:00 LST on January 23rd. After reaching the surface, these enhanced downdrafts create a stronger outflow from the cloud region to the environment. Then, this stronger outflow creates stronger convergence around the surface after colliding with surrounding warm air around 19:00 LST on January 23rd as also simulated in (Khain et al. 2005; Seifert and Beheng 2006; Tao et al. 2007, 2012; van den Heever and Cotton 2007; Storer et al. 2010; Lee 2011) and diagrammatically described in Fig. 4a (see blue circles for convergence in Fig. 4a). The stronger convergence leads to the development of stronger updrafts around 21:00 LST on January 23rd in the 10M run than in the control run (Fig. 8).
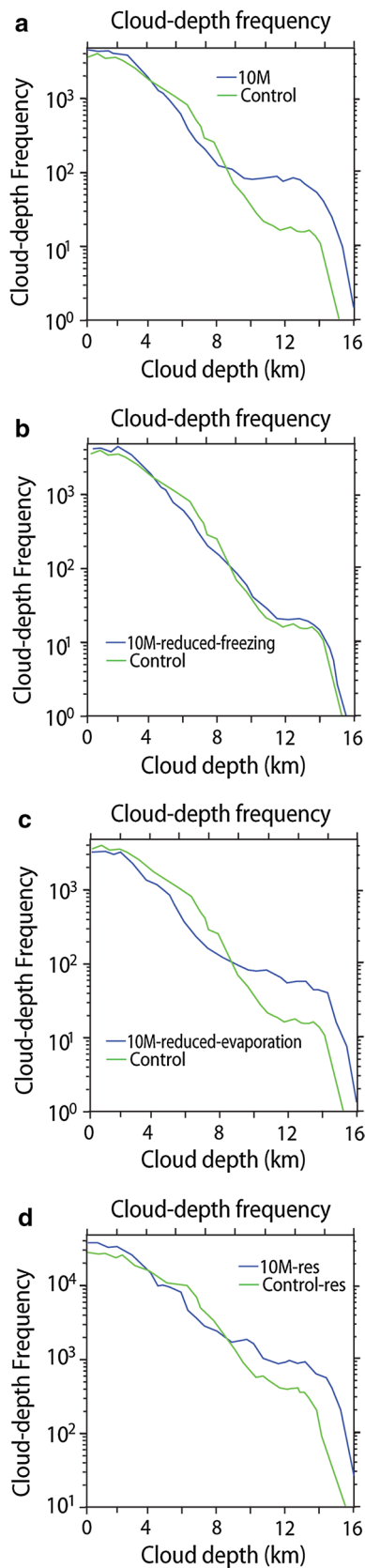
Fig. 6 Distributions of cloud-depth frequency for **a** the 10M and control runs, **b** the 10M-reduced-freezing and control runs, **c** the 10M-reduced-evaporation and control runs and **d** the 10M-res and control-res runs
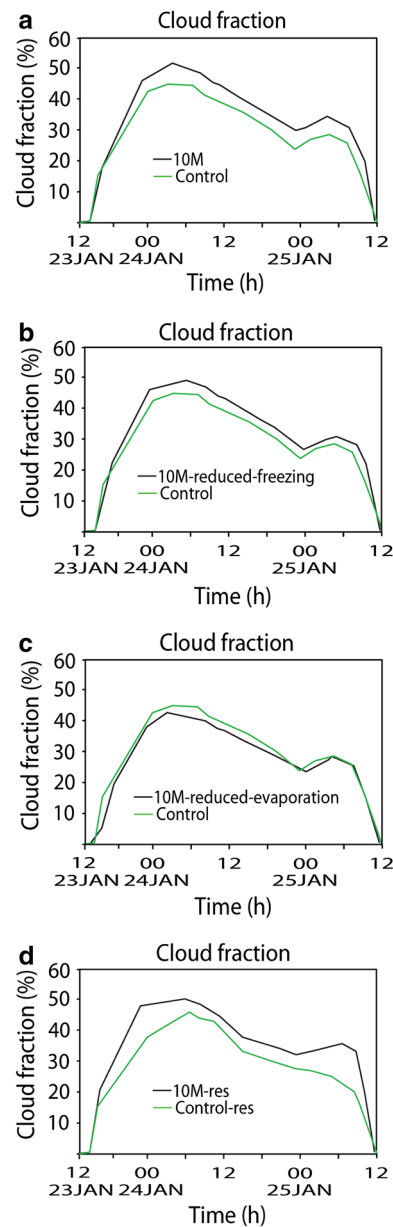
Fig. 7 Time series of cloud fraction for **a** the 10M and control runs, **b** the 10M-reduced-freezing and control runs, **c** the 10M-reduced-evaporation and control runs, and **d** the 10M-res and control-res runs

Figure 9 shows the vertical distribution of evaporation rates averaged over the domain and over the period between the beginning of the simulations and 18:00 LST on January 23rd when downdrafts become stronger in the 10M run than in the control run. There is overall much larger evaporation (and thus evaporative cooling) in the 10M run than in the control run, which leads to larger intensity of downdrafts and convergence in the 10M run than in the control run.

Figure 10a and b show the convergence at the surface and column-averaged condensation rates at 21:15 LST
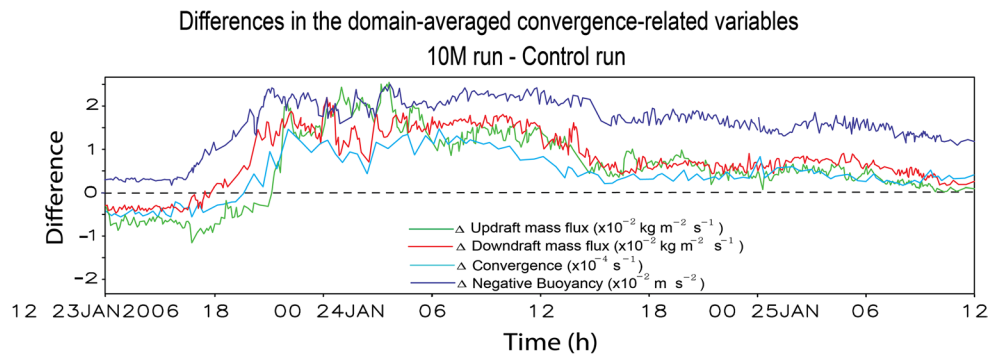
Fig. 8 Time series of differences in the domain-averaged convergence at the surface, the domain-averaged updraft mass fluxes, negative buoyancy that is associated with evaporative cooling and the downdraft mass fluxes between the 10M run and the control run
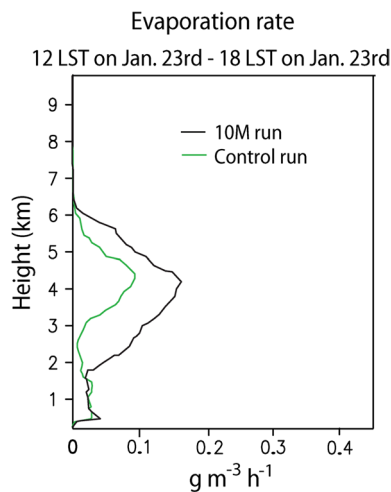
Fig. 9 Vertical distributions of the time- and domain-averaged evaporation rates over the period between 12:00 and 18:00 LST on January 23rd for the 10M and control runs

on January 23rd, which is ~15 min after updrafts become stronger in the 10M run than in the control run. In these figures, each condensation entity with non-zero condensation rates represents a cloud cell. In Fig. 10a and b, there is larger domain-averaged convergence in the 10M run than in the control run. This in turn leads to a situation where there are more air parcels that rise up from the convergence field and thus more condensation entities (or cloud cells) in the 10M run than in the control run (Fig. 10a and b). This explains the larger cumulative number of cloud cells (and associated updraft cores) at the last time step in the 10M run. These more numerous condensation entities, or cloud cells, explains the larger time- and domain-averaged condensation rates in the 10M run. As seen in Fig. 10c, with no increases in evaporative cooling, there are smaller domain-averaged convergence and thus less condensation entities or cloud cells in the 10M-reduced-evaporation run than in the control run.

As discussed in previous studies (e.g., Lee and Feingold 2010), the increasing number of cloud cells in turn increases competitions among cloud cells for given large-scale forcings. Since given convective energy sources in the forcings (e.g., low-level humidity and warm air) are divided into more clouds with the increasing competitions, these evaporation-induced more clouds tend to be smaller with smaller cloud depths. This contributes to the increase in the number of small clouds with depths smaller than ~4 km with increasing evaporation (induced by increasing aerosol concentration), which leads to the increase in PF for light precipitation (as represented by Figs. 3 and 6 and diagrammatically depicted in Fig. 4a). Also, aerosol-induced increases in the number of raindrops and decreases in their size enhance the surface-to-volume ratio of raindrops and thus the efficiency of their evaporation as discussed in Zhao and Garrett (2008). This further reduces the size of raindrops and their fall velocity, which further contributes to the increase in PF for light precipitation as aerosol concentration increases.

Medium-depth clouds (having depths between 4 km and 8 km) and high-depth clouds (having depths larger than 8 km) producing medium and heavy precipitation, respectively, are affected by the increasing competitions, since some portion of medium-depth and high-depth clouds turns into small-depth clouds (with depth smaller than 4 km). This contributes to the increases in the number of small-depth clouds associated with light precipitation in tandem with the increases in the number of small-depth clouds themselves with the increasing evaporation. Also, it is notable that some portion of high-depth clouds can turn into medium-depth clouds with increasing aerosol and evaporation. This contributes to a situation where differences in PF and cloud-depth frequency for medium-depth and high-depth clouds and medium and heavy precipitation between the 10M and control runs are different from those between the 10M-reduced-evaporation run and control run (Figs. 3 and 6). However, qualitative differences in the frequency distributions for medium and high clouds

Fig. 10 The superposition of vertically averaged condensation rate (g m^{-3} s^{-1}) and convergence field (s^{-1}) at the surface at 21:15 LST on January 23rd for **a** the control run, **b** the 10M run, and **c** the 10M-reduced-evaporation run

a

Convergence and condensation
Control run

$\left|\dfrac{\partial u}{\partial x}\right| = 7.5 \times 10^{-4} s^{-1}$ Domain-averaged condensation: $1.86 \times 10^{-4} gm^{-3}s^{-1}$

b

10M run

$\left|\dfrac{\partial u}{\partial x}\right| = 8.1 \times 10^{-4} s^{-1}$ Domain-averaged condensation: $2.96 \times 10^{-4} gm^{-3}s^{-1}$

c

10M-reduced-evaporation run

$\left|\dfrac{\partial u}{\partial x}\right| = 7.3 \times 10^{-4} s^{-1}$ Domain-averaged condensation: $1.80 \times 10^{-4} gm^{-3}s^{-1}$
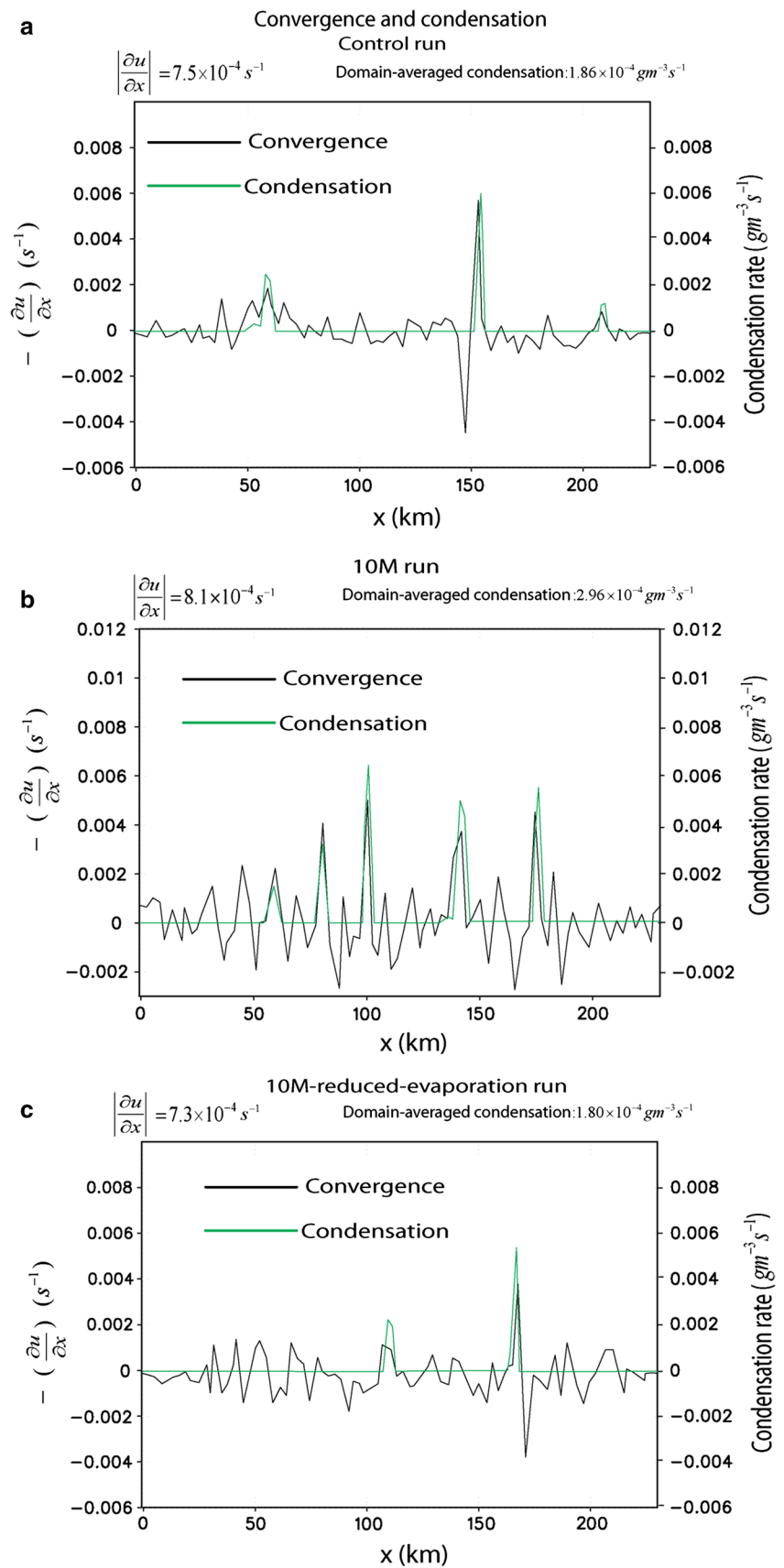
and precipitation between the 10M and the control runs are not different from those between the10M-reduced-evaporation run and the control run (Figs. 3 and 6). Hence, the qualitative differences in medium and high clouds and precipitation between the 10M and control runs are not sensitive to the changing competitions among clouds.

Note that comparisons between Fig. 6a and c show that there are aerosol- and evaporation-induced ~50 % changes in the number of small-depth clouds. The number of small-depth clouds and its changes here are all in the order of ~10^3. These comparisons also show that there are aerosol- and evaporation-induced ~20 % changes in the number of medium-depth and high-depth clouds, which is partially explained by the transition of those clouds to small-depth clouds via aerosol-induced increases in the competitions. Note that the number of medium-depth and high-depth clouds and its changes are mostly in the order of smaller than ~10^3. This indicates that competition-induced transition of medium-depth and high-depth clouds to small-depth clouds accounts for a very small portion of aerosol-induced changes in the number of small-depth clouds. Hence, the increases in the number of small-depth clouds in the 10M run are mainly controlled by the increases in the number of small-depth clouds themselves.

4.2.6 More discussion of aerosol-induced occurrences of extremely heavy precipitation

The small-depth clouds (with depths below ~4 km) do not have enough parts above the level of freezing (~3.5 km) and thus the overall responses of the small-depth clouds to increases in aerosol concentration are controlled by aerosol effects on evaporation, gust fronts and associated competitions among clouds but not by aerosol effects on freezing and buoyancy. However, medium-depth clouds and high-depth clouds (with depths larger than ~4 km) have their much larger portion above the level of freezing as compared to small-depth clouds. Moreover, the responses of these medium-depth clouds and high-depth clouds to increases in aerosol concentration are not sensitive to aerosol-induced increases on evaporation, gust fronts and associated competitions among clouds as strongly as those of small-depth clouds as explained in Sect. 4.2.5. This enables the effect of aerosol-induced increases in buoyancy by aerosol-induced increases in freezing, cloud-bottom convergence and condensation on those medium-depth and deep clouds to be very effective, to be not damped down much (by increases in the competitions among clouds) and thus, to contribute to the full growth or invigoration of some of those clouds. This eventually leads to a situation where some of those clouds grow extremely well (though intermittently) for the occurrence of intermittent extremely heavy precipitation with rates above ~28 mm h^{-1}.
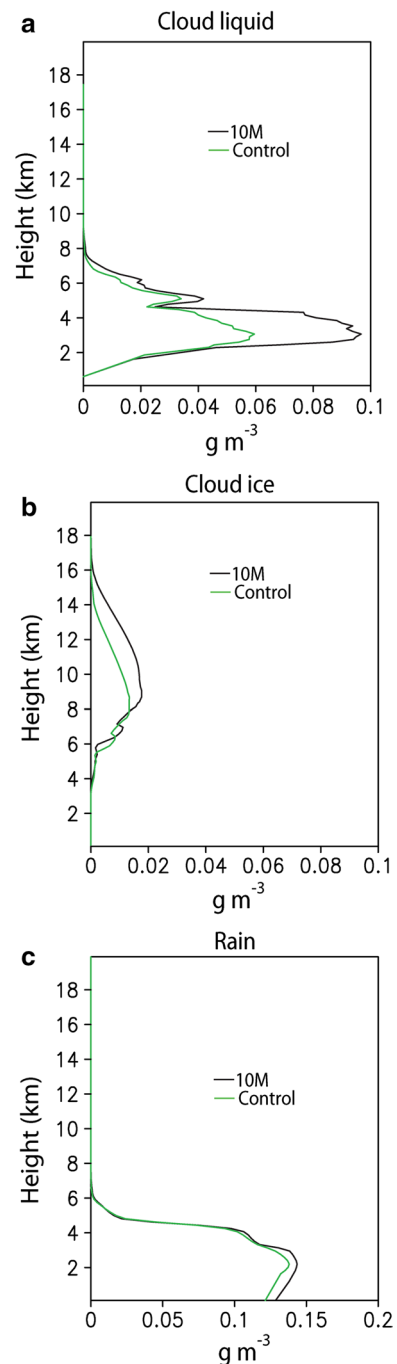
Fig. 11 Vertical distributions of the time- and domain-averaged mass densities of **a** cloud liquid, **b** cloud ice and **c** rain

4.3 Vertical distributions of hydrometeor mass densities

As seen in Fig. 11a showing the time- and domain-averaged vertical profiles of cloud-liquid mass density, the maximum value of this profile is located around 3 km for both the 10M run and the control run. However, the maximum

value is ~70 % larger in the 10M run than in the control run, which is associated with the enhanced intensity of the averaged updrafts with the increasing aerosol concentration as described above.

It is important to note that the location and magnitude of the maximum value in Fig. 11a is not mainly determined by a microphysical factor (i.e., decreasing cloud-liquid particle size with an increasing aerosol concentration) but by "dynamic responses" or "the responses of gust fronts, buoyancy, updrafts and condensation" to the increase in aerosol concentration. If the maximum value is solely controlled by the microphysical factor, the decreasing size or mass of individual cloud-liquid particles with the increasing aerosol concentration leads to an increasing altitude where the maximum value of cloud-liquid mass density occurs as diagrammatically described in Fig. 4c. This is because cloud particles with smaller sizes have smaller fall velocities (Pruppacher and Klett 1997) and thus those particles tend to stay higher in altitude by falling down slower (Fig. 4c).

The increasing aerosol concentration does not change the altitudes of gust fronts in the planetary boundary layer, since the increasing aerosol concentration does not change the altitude of cold air spreading out toward surrounding warm air to form gust fronts as diagrammatically depicted in Fig. 4a. Whether aerosol concentration is high or not, the cold air and downdrafts always spread out at similar altitudes just above the surface when they contact the surface and are not able to penetrate it so that the altitudes of gust fronts in parent clouds, maximum gust-front-induced updrafts, and associated maximum condensation and cloud-liquid mass in subsequent clouds around or just above the gust fronts do not change much with the varying aerosol concentration as depicted in Figs. 4a and 11a.

Another point to make is that cloud liquid or droplets reach places immediate below the level of homogeneous freezing around 9 km with the temperature of ~−38 °C in both the control run and 10M run as seen in Fig. 11a. Note that homogeneous freezing occurs when temperature goes down to −38 °C. As simulated by Phillips et al. (2002, 2007b), Khain et al. (2005, 2008), Lee et al. (2008a, 2009) and Fan et al. (2013), whether aerosol concentration is high or low, generally, in deep convective clouds (simulated in this study) where there are relatively strong updrafts, the transportation of droplets occurs up to the level of homogeneous freezing efficiently and this enables the presence of droplets up to ~9 km in both of the runs.

As seen in Fig. 12a and as diagrammatically depicted in Fig. 4a, homogeneous freezing of droplets and haze particles (unactivated aerosol particles) produce the largest cloud-ice number concentration around the level of the homogeneous freezing (which is around 9 km). The largest cloud-ice number concentration provides the largest sum of
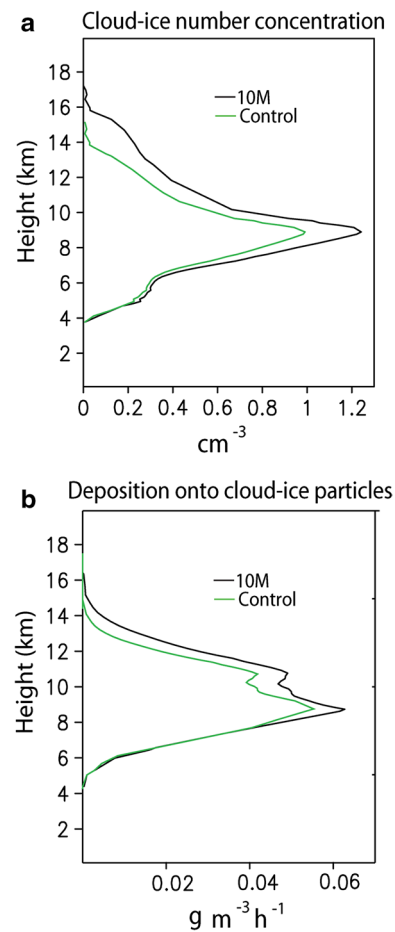
Fig. 12 Vertical distributions of **a** the averaged cloud-ice number concentration over areas and time with non-zero cloud-ice number concentration and **b** the time- and domain-averaged rates of deposition of water vapor onto cloud-ice particles

areas of cloud-ice or ice-crystal surface where deposition of water vapor occurs in a given unit volume of air around 9 km. This induces the largest deposition (or freezing based on the definition of freezing including deposition here) as shown in Fig. 12b through positive feedbacks between updrafts, supersaturation and deposition and produces the maximum cloud-ice mass density around 9 km as shown in Fig. 11b. These feedbacks for the largest deposition or freezing at the level of homogeneous freezing are also simulated in Phillips et al. (2002, 2007b), Khain et al. (2005), Lee et al. (2008a, 2009) and Fan et al. (2013).

If we consider aerosol-induced change in the size of ice-crystal particles only, which is the microphysical factor, the maximum cloud-ice mass density should occur at a higher altitude in the 10M run than in the control run (as explained above and diagrammatically described in Fig. 4c), which is contrary to the results here. Increasing number of droplets and haze particles enhance homogeneous freezing (including associated deposition and explaining most of cloud-ice

Table 2 Time- and domain-averaged production and loss rates of processes related to rain at the altitude of 3 km

Process rates related to rain mass ($g\ m^{-3}\ h^{-1}$)	Control run	10M run
Microphysical source		
Autoconversion	8.57×10^{-5}	3.25×10^{-5}
Accretion of cloud liquid by rain	8.44×10^{-3}	1.45×10^{-2}
Melting of graupel	2.11×10^{-3}	3.40×10^{-3}
Melting of snow	5.10×10^{-4}	6.80×10^{-4}
Microphysical sink		
Rain evaporation	9.77×10^{-4}	9.89×10^{-4}
Accretion of rain by graupel	0.00	0.00
Accretion of rain by snow	0.00	0.00
Contact freezing of rain	0.00	0.00
Accretion of rain by cloud ice	0.00	0.00
Net sedimentation and advection	3.11×10^{-5}	3.34×10^{-5}

particle formation) and associated cloud-ice mass with the increasing aerosol concentration around the level of homogeneous freezing by intensifying the dynamic feedbacks involving updrafts. With the changing aerosol concentration, the altitude of $\sim -38\ °C$ does not change much, since the location of $\sim -38\ °C$ is mainly determined by large-scale forcings but not by aerosol. Hence, although homogeneous freezing (and associated deposition) and thus cloud-ice mass increase, their location and thus the location of the maximum freezing and cloud-ice mass do not vary significantly (despite the decreasing cloud-ice particle size with the increasing aerosol concentration) as seen in Fig. 11b.

Table 2, showing the time- and domain-averaged production and loss rates of processes related to rain at 3 km, indicates that accretion of cloud liquid by rain is the primary factor for the maximum values of rain mass at 3 km as shown in Fig. 11c. The secondary factor is melting of graupel, reflecting the fact that 3 km is around the level of freezing or melting. As seen in Fig. 11c, there is overall slightly larger rain mass density in the 10M run than in the control run with negligible changes in the altitude of the maximum rain mass between the runs. The slightly larger rain mass in the 10M run particularly at 3 km is mainly a result of aerosol-enhanced accretion of cloud liquid by precipitation as shown in Table 2. Aerosol-induced changes in raindrop size and thus the terminal velocity of raindrops, which are changes in microphysical factors, should result in different altitudes of the maximum rain mass between the runs. Since accretion of cloud liquid by precipitation is primarily controlled by cloud-liquid mass that acts as the most important source of accretion, despite aerosol-induced changes in raindrop size, the altitude of maximum rain mass for both the 10M run and the control run is around 3 km (Fig. 11c). Note that 3 km is the altitude where the

maximum cloud-liquid mass occurs through the gust fronts and associated updrafts (Fig. 11a). This again demonstrates that the altitude and magnitude of the maximum rain mass is determined by updraft or dynamic responses (involving gust fronts) to the increase in aerosol concentration but not by the responses of microphysical factors.

Our analysis of the very first time step of rain formation for each of the 10M and control runs shows that initial rain forms at lower altitudes around 90 min earlier in the control run than in the 10M run. In the control run, the altitude of the initial formation of rain is ~600 m, while the altitude is ~1200 m in the 10M run. This is because larger cloud-liquid particles in the control run than in the 10M run enable themselves to start to convert into rain particles via autoconversion in the control run, although air parcels in the control run carrying those cloud-liquid particles and originated from around the surface do not reach altitudes as high as those in the 10M run. Note that larger cloud-liquid particles have higher efficiencies of collecting each other at their collision, which enables the earlier growth of cloud-liquid particles to raindrops via the collection with smaller aerosol concentration than with higher aerosol concentration (Rogers and Yau 1991; Pruppacher and Klett 1997). The earlier initial formation of raindrop and the lower altitudes of initial raindrop formation in the control run (caused by autoconversion difference, which is a microphysical factor) enable raindrops to reach the surface earlier and thus enable precipitation amount at the surface to start to be accumulated earlier. This is in favor of longer duration of the surface precipitation and thus raising the possibility of a higher total precipitation amount in the control run than in the 10M run. However, total precipitation amount is slightly larger in the 10M run due to the dynamic responses to the increasing aerosol concentration.

5 Discussion

5.1 Comparisons with other studies

Previous studies (e.g., van den Heever et al. 2011; Li et al. 2011; Wang et al. 2011; Fan et al. 2012; Koren et al. 2012) examined the response of PF to aerosol in MCE. Note that while van den Heever et al. (2011), Wang et al. (2011) and Fan et al. (2012) relied on models for the PF calculation, Li et al. (2011) and Koren et al. (2012) used satellite and ground-based observations for their calculations. The maximum R in those studies is not only different between them but also different from this study, as are the classifications into R ranges. The significantly different classifications exacerbate comparisons among the studies. Nevertheless, there is a good agreement amongst the above-mentioned studies and this study that an increase in aerosol enhances

the frequency of relatively heavy precipitation. However, in other ranges of R (for relatively light precipitation), there are discrepancies in the response of PF. This may not be that surprising considering significant differences in the development stages of convection and environmental conditions among studies and the strong dependence of cloud and precipitation characteristics on these conditions and stages (Weisman and Klemp 1982; Houze 1993; Lynn et al. 2005a, b; Khain et al. 2005, 2008; Lee et al. 2008b; Fan et al. 2009; Khain 2009; Lee 2011; Tao et al. 2012).

Note that evaporation is strongly dependent on wind shear among environmental conditions (e.g., wind shear, stability and humidity) which controls the efficiency of the transportation of cloud liquid (or droplets) and raindrops to unsaturated areas and thus that of cloud-liquid and rain evaporation. Wind shear varies a lot with increasing latitudes from tropics to high-latitude regions through mid-latitude regions. Hence, this can lead to a different efficiency of evaporation and thus intensification of gust fronts by an aerosol perturbation among different regions, which can be one of the reasons why there are differences in PF responses to aerosol for relatively light precipitation among the studies. Motivated by this, the 10M run and the control run are repeated with different wind shear.

The first set of the repeated runs (referred to as "the 10M-small-ws run" and the "control-small-ws run") adopts smaller wind shear, while the second set of repeated runs (referred to as "the 10M-large-ws run" and the "control-large-ws run") adopts larger wind shear as compared to that in the 10M run and the control run. The wind shear is defined as the difference between the density-weighted mean wind speed over the lowest 6 km of the wind profile and the average wind speed over the lowest 500 m of the wind profile, following the definition of Weisman and Klemp (1982). To apply smaller wind shear to the "the 10M-small-ws run" and the "control-small-ws run", the speed of horizontal background wind (which is mostly eastward) above 500 m is reduced by a factor of 2 as compared to that in the 10M run and the control run. To apply larger wind shear to the "the 10M-large-ws run" and the "control-large-ws run", the speed of horizontal wind above 500 m is enhanced by a factor of 2 as compared to that in the 10M run and the control run.

Due to the lower (higher) efficiency of the transportation of cloud liquid to unsaturated areas with smaller (larger) wind shear, aerosol-induced intensification of gust fronts is weaker (stronger) between the control-small-ws run (control-large-ws run) and the 10M-small-ws run (10M-large-ws run) than between the 10M run and the control run. This leads to a situation where the 10M-small-ws run shows smaller PFs for light precipitation (with rates below 5 mm h^{-1}) than the control-small-ws run, while the 10M-large-ws run shows larger PFs for light precipitation

than the control-large-ws run and the difference in those PFs (for light precipitation) between the 10M-large-ws run and the control-large-ws run is larger than that between the 10M run and the control run (Fig. 3a, e and f). These repeated runs with the different sets of wind shear demonstrate that the response of PF for light precipitation to aerosol perturbations is strongly dependent on wind shear which is one of representative environmental conditions. This gives us a preliminary clue to a reason why the response of the relatively light precipitation to aerosol perturbations varies among studies over different regions.

5.2 Scavenging

Although aerosol concentration and its difference between the 10M and control runs decrease with time, the feedbacks involving aerosol-induced increases in freezing, cloud-bottom convergence, evaporation, the intensity of gust fronts and condensation are established at the beginning stage of cloud development. The beginning stage is much before cloud development reaches its mature stage when strong precipitation occurs and thus the scavenging is most effective; remind that using experiments and measurements, Garrett et al. (2010), Pruppacher and Klett (1997), and Shaw (1995) have shown that higher precipitation rates induce higher scavenging. In other words, those feedbacks are set up at the beginning stage when there are weak precipitation and thus no significant effects of scavenging on aerosol concentration and its difference between the runs. Those feedbacks set up at the beginning stage determine the differences in cloud and precipitation development regardless of the evolution of the differences in aerosol concentration between the runs even after the beginning stage. Hence, results here are quite robust to the effect of scavenging on differences in aerosol concentration between the two runs as also extensively discussed in (Lee et al. 2008a, b; Lee and Feingold 2010; Lee 2011; Lee and Feingold 2013).

5.3 Sensitivity to resolutions and dimensionality

The features of simulated MCEs can vary with varying resolutions (e.g., Sato et al. 2008; Donner et al. 1999). To examine the sensitivity of results here to resolutions, the 10M run and the control run are repeated with a horizontal grid length of 100 m (reduced from 500 m) and a vertical grid length of 50 m (reduced from 200 m) that are generally adopted by large-eddy simulation (LES) modeling. These repeated runs are referred to as the 10M-res run and the control-res run, respectively. For these repeated runs, the length of the horizontal domain is reduced from 256 km to 100 km to save the computational cost. This reduction in the length of the horizontal domain is based on the fact

that the size or horizontal extent of individual convection is generally 5–30 km and it is much smaller than 100 km. Hence, we believe that the reduced domain size has a minimal impact on the development of individual convection or individual clouds. Also, Houze (1993) defined a mesoscale convective system (or MCE) as a cloud system that occurs in connection with an ensemble of thunderstorms and produces precipitation area ~100 km or more in at least one direction. Hence, the 100-km length captures the MCE and its mesoscale structure as the 256-km domain length for the standard runs does. Moreover, Phillips and Donner (2007) have compared results obtained by averaging an ensemble of 85 small (~100 km) domains to those from a single large (~5000 km) domain and found that their statistical behaviors are similar, due to the fact that the size of individual convection is much smaller than the size of the domain whether it is a 100-km small domain or a 5000-km large domain. This supports the use of 100-km length to test the effect of resolutions on the results here. Figures 3g, 6d and 7d for precipitation frequency, cloud-depth frequency, and cloud fraction from these repeated runs and comparisons between these figures and Figs. 3a, 6a and 7a from the 10M and control runs demonstrate that the qualitative nature of results is insensitive to resolutions.

For simulations of observed MCEs over the Southern Great Plains (SGP), Lee et al. (2008a, b) have shown that aerosol-induced intensification of updrafts and the qualitative nature of the response of PF to increasing aerosol concentration for each of light, medium and heavy precipitation are robust to whether two-dimensional domain or three-dimensional domain is selected. Note that the intensification of updrafts is a good manifestation of the effects of aerosol on dynamics (and associated microphysics) described in Lee et al. (2008a, b) and this study. This is because the updraft can be considered to be a final product of what has been going on in dynamic situation (including the intensity of gust fronts) of cloud systems. These MCEs over the SGP involve various types of clouds from shallow warm clouds to deep clouds that reach the tropopause as the MCE simulated in this study does. There are similar responses of PF to aerosol perturbations between the MCEs over the SGP and the MCE simulated in this study for each of light, medium and heavy precipitation. This enables a reasonable comparison between the MCEs over the SGP and the MCE simulated here for the matter of dimensionality. Hence, although simulations in Lee et al. (2008a, b) are for different cases, they suggest that the qualitative character of results presented here is not caused by the two-dimensional domain.

5.4 Sensitivity to sublimation

This study put its emphasis on aerosol-induced changes in freezing and evaporation and their impacts on PF.

However, this does not mean that there are no other potential microphysical processes which affect PF. For example, Fan et al. (2008), Wang et al. (2011), and Tao et al. (2012) have shown that sublimation can have impacts on convection and precipitation by controlling latent cooling, downdrafts and gust fronts. Motivated by this, the 10M run is repeated with reduced sublimation by a factor of 2. This makes cumulative sublimation in the repeated run identical to that in the control run. This repeated run is referred to as the "10M-reduced-sublimation run". Comparisons of PF between the 10M-reduced-sublimation run and the control run show results that are qualitatively similar to those between the 10M run and the control run (Fig. 3a and h). Hence, aerosol-induced increases in sublimation do not contribute to the qualitative differences in PF between the 10M run and the control run.

6 Summary and conclusions

This study finds that aerosol-induced increases in freezing (and parcel buoyancy) mostly enhance PF which is associated with heavy rain from deep clouds with R above ~15 mm h^{-1}. This accompanies extremely heavy precipitation with R larger than ~28 mm h^{-1} which does not exist in the absence of aerosol-induced increases in freezing. This study also finds that aerosol-induced increases in evaporation have a significant impact on PF associated with light and medium rain with R below ~15 mm h^{-1} which is produced by small- and medium-depth clouds with depths below ~8 km. The effect of aerosol-induced increases in evaporation on small- and medium-depth clouds and associated precipitation has also been discussed in (Xue and Feingold 2006; Feingold et al. 2010; Lee et al 2012), although this effect has been often neglected in studies of interactions between convective clouds and aerosol. In particular, for light precipitation with rates smaller than 5 mm h^{-1}, the increase in evaporation is the cause of larger PFs in the high-aerosol case than in the low-aerosol case. Aerosol-induced increases in evaporation increase the number of clouds and competitions among them and reduce the size of raindrops and their fall velocity, which contribute to the more small-depth clouds and the more light precipitation. Eventually, the increase in the light-rain PF induced by aerosol enables the larger cumulative precipitation in the high-aerosol case than in the low-aerosol case. With no increase in evaporation and light rain, aerosol-induced suppression of precipitation amount is simulated in the high-aerosol case.

Sensitivity tests have demonstrated that aerosol-induced changes in PF for light precipitation are sensitive to the magnitude of wind shear. This can explain the reason why the response of PF to aerosol perturbations varies widely

with varying regions and thus varying environmental conditions. However, it is true that the level of understanding of the variation is still very low, since there are other environmental factors than wind shear that may contribute to the variation of the response of PF to aerosol perturbations. Hence, further examination of the variation to better understand the cause of the discrepancies in the PF responses to aerosol perturbations among studies in different regions is worthy of future research efforts.

This study shows that extremely heavy precipitation with rate above ~28 mm h^{-1} is created by aerosol perturbation that affects freezing. This extremely heavy precipitation is related to extreme weather events such as flash flooding and has important implications for us socially and economically. This indicates that parameterizations of aerosol and ice microphysical processes (e.g., freezing) are crucial to better simulate or trigger extreme weather events related to flooding in climate and regional models.

The locations of gust fronts and associated condensation and those of homogeneous freezing and associated deposition do not vary much with varying aerosol concentration and this outweighs the effect of changing cloud-particle size on the locations or altitudes of the maximum values of the averaged rain, cloud-liquid and –ice mass. This leads to the negligible variation of the altitudes of the maximum values with varying aerosol concentration. Despite the earlier formation of precipitation and its lower altitude, precipitation amount is slightly smaller in the control run than in the 10M run due to dynamic responses (involving updrafts and gust-front responses) to aerosol. This indicates that aerosol-induced changes in microphysical factor (e.g., cloud-particle size) itself are not able to explain results (e.g., the responses of cumulative precipitation and the altitudes of the maximum values of the averaged mass to aerosol) shown in this paper. To better explain them, work in this paper demonstrates that we have to consider cloud dynamics (involving updrafts and gust fronts), temperature vertical profiles (affecting processes such as homogeneous freezing) and associated phase-transition and latent-heat processes.

In general, aerosol community tends to think about aerosol-cloud interactions in convective clouds as those involving aerosol-induced increases in freezing, cloud-top heights and precipitation amount without being concerned about changes in cloud-system organization and the spatiotemporal distributions of precipitation. This tendency is based on studies of single-cloud systems (Rosenfeld and Woodley 2000; Rosenfeld et al. 2008). This study makes a contrast between the freezing effect which acts as a basis for the concept based on single-cloud systems and the evaporation effect which is accepted as a primary driver of aerosol-induced changes in cloud-system organizations in multiple-cloud systems. This contrast can shed light on

the importance of the consideration of other processes and associated changes in cloud-system organizations in addition to freezing and cloud-top height.

We believe that not many previous studies have been successfully explaining aerosol-induced changes in cloud systems by relying only on either freezing or evaporation. Thus this study, looking at both freezing and evaporation, acts as a first stepping stone to a comprehensive understanding of aerosol-cloud interactions in convective cloud systems. Considering that multiple-cloud systems play a much more important role in climate than a single cloud (Houze 1993), this type of comprehensive understanding gives us clearer insight into roles played by aerosol-cloud interactions in climate.

References

Abdul-Razzak H, Ghan SJ (2000) A parameterization of aerosol activation 2. Multiple aerosol types. J Geophys Res 105:6837–6844

Abdul-Razzak H, Ghan SJ (2002) A parameterization of aerosol activation—3. Sectional representation. J Geophys Res 107:4026. doi:10.1029/2001JD000483

Albrecht BA (1989) Aerosols, cloud microphysics, and fractional cloudiness. Science 245:1227–1230

Donner LJ, Seman CJ, Hemler RS (1999) Three-dimensional cloud-system modeling of GATE convection. J Atmos Sci 56:1885–1912

Fan J, Zhang R, Tao WK, Mohr K (2008) Effects of aerosol optical properties on deep convective clouds and radiative forcing. J Geophys Res 113:D08209. doi:10.1029/2007JD009257

Fan J, Yuan T, Comstock JM, Ghan SJ, Khain A, Leung LYR, Li Z, Martins VJ, Ovchinnikov M (2009) Dominant role by vertical wind shear in regulating aerosol effects on deep convective clouds. J Geophys Res. doi:10.1029/2009JD012352

Fan J, Leung LR, Li Z et al (2012) Aerosol impacts on clouds and precipitation in eastern China: results from bin and bulk microphysics. J Geophys Res 117:D00K36. doi:10.1029/2011JD016537

Fan J, Leung LR, Rosenfeld D et al (2013) Microphysical effects determine macrophysical response for aerosol impacts on deep convective clouds. Proc Natl Acad Sci USA 110:E4581–E4590. doi:10.1073/pnas.1316830110

Feingold G, Koren I, Wang H, Xue H, Brewer A (2010) Precipitation-generated oscillations in open-cellular cloud fields. Nature 466:849–852

Fridlind A et al (2009) ARM/GCSS/SPARC TWP-ICE intercomparison study. http://science.arm.gov/wg/cpm/scm/scmic6/index.html

Garrett TJ, Zhao C (2006) Increased Arctic cloud longwave emissivity associated with pollution from mid-latitudes. Nature 440:787–789

Garrett TJ, Zhao C, Novelli PC (2010) Assessing the relative contributions of transport efficiency and scavenging to seasonal variability in Arctic aerosol. Tellus B. 62:190–196. doi:10.1111/j.1600-0889.2010.00453.x

Houze RA (1993) Cloud dynamics. Academic Press, London

Khain AP (2009) Notes on state-of-the-art investigations of aerosol effects on precipitation: a critical review. Environ Res Lett. doi:10.1088/1748-9326/4/1/015004

Khain A, Rosenfeld D, Pokrovsky A (2005) Aerosol impact on the dynamics and microphysics of deep convective clouds. Q J R Meteorol Soc 131:2639–2663

Khain A, Benmoshe N, Pokrovsky A (2008) Factors determining the impact of aerosols on surface precipitation from clouds: an attempt at classification. J Atmos Sci 65:1721–1748

Koop T, Luo B, Tsias A, Peter T (2000) Water activity as the determinant for homogeneous ice nucleation in aqueous solutions. Nature 406:611–614

Koren I, Altaratz O, Remer LA et al (2012) Aerosol-induced intensification of rain from the tropics to the mid-latitude. Nat Geosci 5:118–122

Lee SS (2011) Dependence of aerosol-precipitation interactions on humidity in a multiple-cloud system. Atmos Chem Phys 11:2179–2196

Lee SS, Feingold G (2010) Precipitating cloud-system response to aerosol perturbations. Res. Lett, Geophys. doi:10.1029/2010GL045596

Lee SS, Feingold G (2013) Aerosol effects on the cloud-field properties of tropical convective clouds. Atmos Chem Phys 13:6713–6726

Lee SS, Donner LJ, Phillips VTJ, Ming Y (2008a) Examination of aerosol effects on precipitation in deep convective clouds during the 1997 ARM summer experiment. Q J R Meteorol Soc. doi:10.1002/qj.287

Lee SS, Donner LJ, Phillips VTJ, Ming Y (2008b) The dependence of aerosol effects on clouds and precipitation on cloud-system organization, shear and stability. J Geophys Res 113:D16202. doi:10.1029/2007JD009224

Lee SS, Donner LJ, Phillips VTJ (2009) Sensitivity of aerosol and cloud effects on radiation to cloud types: comparison between deep convective clouds and warm stratiform clouds over one-day period. Atmos Chem Phys 9:2555–2575

Lee SS, Donner LJ, Penner JE (2010) Thunderstorm and stratocumulus: how does their contrasting morphology affect their interactions with aerosols? Atmos Chem Phys 10:6819–6837. doi:10.5194/acp-10-6819-2010

Lee SS, Feingold G, Chuang PY (2012) Effect of aerosol on cloud–environment interactions in trade cumulus. J Atmos Sci 69:3607–3632

Li Z, Niu F, Fan J et al (2011) Long-term impacts of aerosols on the vertical development of clouds and precipitation. Nature Geosci 4:888–894

Lohmann U, Diehl K (2006) Sensitivity studies of the importance of dust ice nuclei for the indirect aerosol effect on stratiform mixed-phase clouds. J Atmos Sci 63:968–982

Lynn B, Khain A, Dudhia J, Rosenfeld D, Pokrovsky A, Seifert A (2005a) Spectral (bin) microphysics coupled with a mesoscale model (MM5). Part 1. Model description and first results. Mon Weather Rev 133:44–58

Lynn B, Khain A, Dudhia J, Rosenfeld D, Pokrovsky A, Seifert A (2005b) Spectral (bin) microphysics coupled with a mesoscale model (MM5). Part 2: simulation of a CaPE rain event with squall line. Mon Weather Rev 133:59–71

May PT, Mather JH, Vaughan G, Jakob C (2008) Characterizing oceanic convective cloud systems—the tropical warm pool international cloud experiment. Bull Am Meteorol Soc 154:153–155. doi:10.1175/BAMS-89-2-153

Mellor GL, Yamada T (1982) Development of a turbulence closure model for geophysical fluid problems. Rev Geophys 20:851–875

Möhler O, Field PR, Connolly P, Benz S, Saathoff H, Schnaiter M, Wagner R, Cotton R, Krämer M, Mangold A, Heymsfield AJ (2006) Efficiency of the deposition mode ice nucleation on mineral dust particles. Atmos Chem Phys 6:3007–3021. doi:10.5194/acp-6-3007-2006

Phillips VTJ, Donner LJ (2007) Cloud microphysics, radiation, and vertical velocities in two- and three-dimensional simulations of deep convection. Q J R Meteorol Soc 133:3011–3033

Phillips VTJ, Choularton T, Blyth A, Latham J (2002) The influence of aerosol concentrations on the glaciation and precipitation of a cumulus cloud. Q J R Meteorol Soc 128:951–971

Phillips VTJ, Donner LJ, Garner S (2007a) Nucleation processes in deep convection simulated by a cloud-system-resolving model with double-moment bulk microphysics. J Atrmos Sci 64:738–761

Phillips VTJ, Pokrovsky A, Khain A (2007b) The influence of time-dependent melting on the dynamics and precipitation production in maritime and continental storm clouds. J Atmos Sci 64:338–359

Pruppacher HR, Klett JD (1997) Microphysics of clouds and precipitation. D. Reidel, Dordrecht

Rogers RR, Yau MK (1991) A short course in cloud physics. Pergamon Press, Oxford

Rosenfeld D, Woodley WL (2000) Convective clouds with sustained highly supercooled liquid water down to −37° C. Nature 405:440–442. doi:10.1038/35013030

Rosenfeld D, Lohmann U, Raga GB et al (2008) Flood or drought, how do aerosols affect precipitation? Science 321:1309–1313

Saleeby SM, Cotton WR (2004) A large-droplet mode and prognostic number concentration of cloud droplets in the Colorado state university regional atmospheric modeling system (RAMS). Part I: module description and supercell test simulations. J Appl Meteorol 43:182–195

Sato T, Yoshikane T, Satoh M et al (2008) Resolution dependency of the diurnal cycle of convective clouds over the Tibetan Plateau in a mesoscale model. J Meteorol Soc Japan 85A:17–31

Seifert A, Beheng KD (2006) A two-moment cloud microphysics parameterization for mixed-phase clouds. Part 2: maritime vs. continental deep convective storms. Meteorol Atmos Phys 92:67–82

Shaw GE (1995) The Arctic haze phenomenon. Bull Am Meteorol Soc 76:2403–2413

Storer RL, van den Heever SC, Stephens GL (2010) Modeling aerosol impacts on convection under differing storm environments. J Atmos Sci 67:3904–3915. doi:10.1175/2010JAS3363.1

Tao W-K et al (2003) Microphysics, radiation and surface processes in the Goddard Cumulus Ensemble (GCE) model. Meteorol Atmos Phys 82:97–137

Tao W-K, Li X, Khain A, Matsui T, Lang S, Simpson J (2007) Role of atmospheric aerosol concentration on deep convective precipitation: cloud-resolving model simulations. J Geophys Res 112:D24S18. doi:10.1029/2007JD008728

Tao W-K, Chen J-P, Li Z, Wang C, Zhang C (2012) Impact of aerosols on convective clouds and precipitation. Rev Geophys 50:RG2001. doi:10.1029/2011RG000369

Twomey S (1977) The influence of pollution on the shortwave albedo of clouds. J Atmos Sci 34:1149–1152

van den Heever SC, Cotton WR (2007) Urban aerosol impacts on downwind convective storms. J Appl Meteorol Climatol 46:828–850. doi:10.1175/JAM2492.1

van den Heever SC, Stephens GL, Wood NB (2011) Aerosol indirect effects on tropical convection characteristics under conditions of radiative-convective equilibrium. J Atmos Sci 68:699–718

Wang Y, Wan Q, Meng W et al (2011) Long-term impacts of aerosols on precipitation and lightning over the Pearl river delta megacity area in China 11:12421–12436

Weisman ML, Klemp JB (1982) The dependence of numerically simulated convective storms on vertical wind shear and buoyancy. Mon Weather Rev 110:504–520

Xue H, Feingold G (2006) Large-Eddy simulations of trade wind cumuli: investigation of aerosol indirect effects. J Atmos Sci 63:1605–1622

Zhao C, Garrett TJ (2008) Ground-based remote sensing of precipitation in the Arctic. J Geophys Res 113:D14204. doi:10.1029/2007JD009222

Zhao C, Klein SA, Xie S, Liu X, Boyle JS, Zhang Y (2012) Aerosol first indirect effects on non-precipitating low-level liquid cloud properties as simulated by CAM5 at ARM sites. Geophys Res Lett 39:L08806. doi:10.1029/2012GL051213